Angle-resolved photoemission and band-structure results for linear chain $TlGaTe_2$

K. Okazaki,[1] K. Tanaka,[1] J. Matsuno,[1] A. Fujimori,[1,2] L. F. Mattheiss,[1] S. Iida,[3] E. Kerimova,[4] and N. Mamedov,[4,*]
[1]*Department of Physics, University of Tokyo, Bunkyo-ku, Tokyo 113-0033, Japan*
[2]*Department of Complexity Science and Engineering, University of Tokyo, Bunkyo-ku, Tokyo 113-0033, Japan*
[3]*Nagaoka University of Technology, Nagaoka, Niigata 940-2188, Japan*
[4]*Institute of Physics, Academy of Sciences, Baku 370143, Azerbaijan*
(Received 4 January 2001; published 3 July 2001)

$TlGaTe_2$ has a quasi-one-dimensional crystal structure consisting of Tl and linked $GaTe_4$ tetrahedral chains. We have studied the electronic band structure of $TlGaTe_2$ by means of photoemission spectroscopy and band-structure calculation. Comparison between both results is rather favorable and energy bands show strong dispersion perpendicular to the chain direction. We have measured the temperature dependence of the spectra and attributed the observed spectral shifts to a downward shift of the Fermi level with decreasing temperature.

DOI: 10.1103/PhysRevB.64.045210 PACS number(s): 71.20.−b, 71.15.Mb, 79.60.−i

I. INTRODUCTION

A series of compounds $TlMX_2$ (M=Ga, In; X=S, Se, Te) have highly anisotropic crystal structures. $TlGaS_2$, $TlInS_2$, and $TlGaSe_2$ have quasi-two-dimensional layered structures and exhibit para-to-ferroelectric phase transitions through an intermediate incommensurate phase. $TlGaTe_2$, $TlInSe_2$, and $TlInTe_2$ have the TlSe-type ($B37$) quasi-one-dimensional chain structure[1] shown in Fig. 1 and exhibit nonlinear transport properties.[2,3] This structure is body-centered tetragonal and features c-axis chains of Tl atoms and edge-sharing $GaTe_4$ tetrahedra. TlSe undergoes a pressure-induced semiconductor-metal transition.[4] Under ambient conditions, the resistivity ratio parallel and perpendicular to the c axis ($\rho_\parallel/\rho_\perp$) of TlSe is ~ 2. Under high pressure, $\rho_\parallel/\rho_\perp$ becomes unity at about 0.6 GPa, decreases continuously, and becomes as low as 0.016 at 5.0 GPa. Both $\rho_\parallel$ and $\rho_\perp$ decrease continuously with pressure and reach metallic values at about 2.7 GPa. According to NMR studies,[5,6] it is suggested that the indirect nuclear spin-spin interaction of Tl isotopes between chains is stronger than that along the chain. Band-structure calculations using the semi-empirical pseudopotential method[7,8] show a dispersion along the direction perpendicular to the chain. According to the x-ray-diffraction study,[9] $TlGaTe_2$ has an incommensurately distorted phase with a reduction of the lattice constant a in going from 290 to 110 K. According to a calorimetric measurement, a second-order structural phase transition occurs at 98.5 K.[9]

So far the anisotropy of the resistivity in $TlGaTe_2$ has not been measured. However, if the electrical resistivities of the TlSe-type compounds have common features with TlSe, the anisotropy of the resistivity in $TlGaTe_2$ may be opposite ($\rho_\parallel/\rho_\perp > 1$) to what would be expected from the chain structure ($\rho_\parallel/\rho_\perp \ll 1$), and one-dimensional behavior may be realized only under high pressure. To understand the anisotropic transport properties of the TlSe-type compounds, it is useful to investigate the electronic band structure experimentally and theoretically. In this paper, we study the electronic band structure of $TlGaTe_2$ by photoemission spectroscopy (PES) and first-principles band-structure calculation, focusing on the anisotropy of the electronic structure.

II. EXPERIMENT

Single crystals were grown by a modified Bridgeman method, as reported previously.[10] Angle-integrated and angle-resolved photoemission (AIPES and ARPES) spectra were measured using a VSW hemispherical analyzer and a VG He discharge lamp. The He I ($h\nu$=21.2 eV) and He II ($h\nu$=40.8 eV) lines were used for excitation. Energy calibration and the estimation of the instrumental resolution were done by measuring the Fermi edge of Au evaporated on the sample manipulator. Clean (110) surfaces were obtained by cleaving the samples *in situ*. We took Laue photographs to confirm the direction of the crystal axis. The energy resolution of AIPES was about 30 meV for He I and about 90 meV for He II. The acceptance angle of the electron analyzer for AIPES was about $\pm 8°$. The angular and energy resolution for ARPES was about $\pm 1°$ and 90 meV, respectively. The take-off angle θ could be varied along only one direction and the accuracy of the emission angle along the other direction was about $\pm(2-3)°$. The measurements were made at 22 K and room temperature. The base pressure in the analyzer chamber was below 1×10^{-10} Torr.

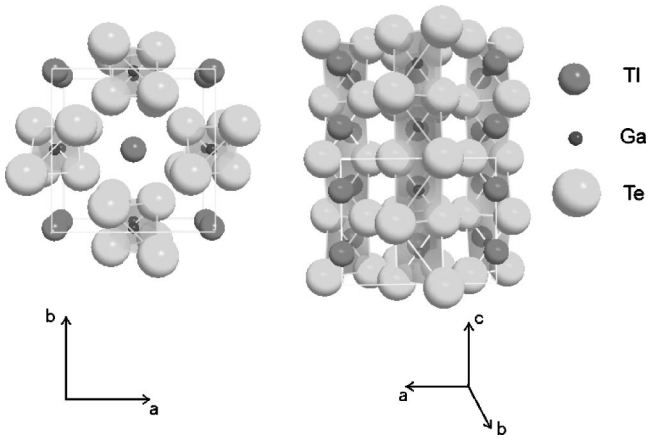

FIG. 1. Crystal structure of $TlGaTe_2$.

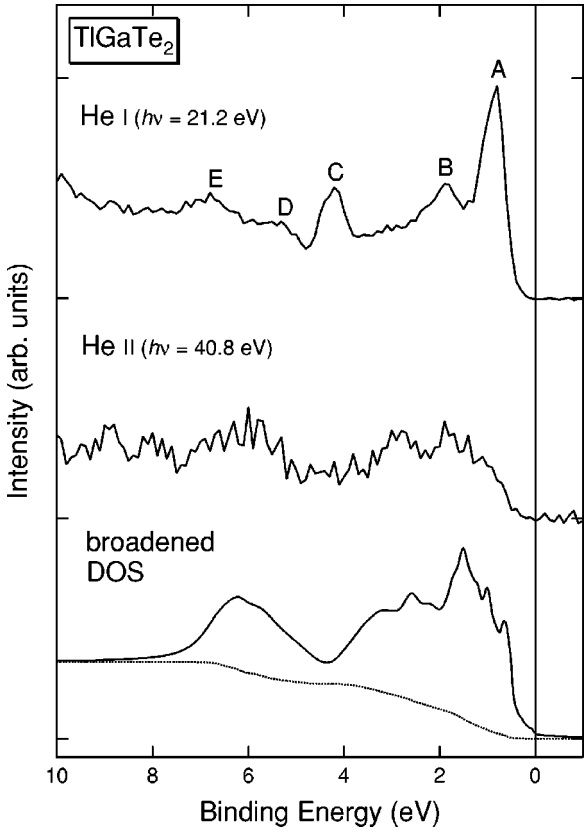

FIG. 2. Comparison of the AIPES spectrum with the calculated DOS. The dotted line shows the integral background.

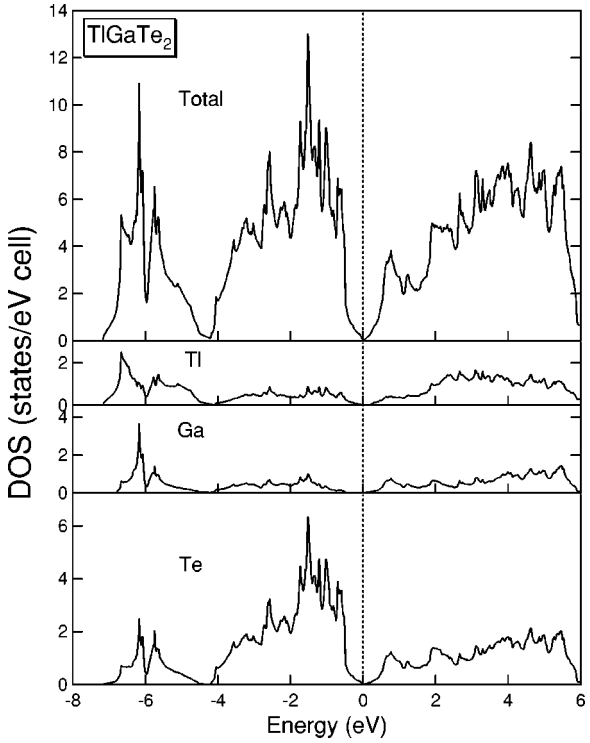

FIG. 3. Total and muffin-tin projected DOS.

III. BAND-STRUCTURE CALCULATION

The body-centered-tetragonal $TlGaTe_2$ structure contains two formula units per unit cell. The structural parameters utilized in the present calculations include the lattice parameters $a=8.429$ Å and $c=6.868$ Å,[12] and the Te atom internal position parameters ($x=0.175$, $y=0.675$) from the structural data for TlSe.[7] These parameters yield a Ga-Te tetrahedral bond length of about 2.70 Å and a Tl-Tl bond length along the *c*-axis chain (3.43 Å) which is only slightly smaller than the 3.55-Å separation between Tl and the Te atoms which make up the $GaTe_4$ tetrahedra.

The present band-structure calculation has been carried out in the local-density approximation (LDA) using a full-potential, scalar-relativistic implementation[11] of the linear augmented plane-wave (LAPW) method.[13] The LAPW basis includes plane waves with a 8-Ry cutoff ($\sim$80 LAPW's/atom) and spherical-harmonic terms up to $l=8$ inside the muffin-tin spheres. The crystalline charge density and potential have been expanded using $\sim$5700 plane waves (35 Ry cutoff) in the interstitial region and lattice harmonics with $l_{max}=6$ inside the muffin-tin spheres ($R_{\mathrm{Tl}}\sim 3.14$ a.u., $R_{\mathrm{Ga}}\sim 2.36$ a.u., $R_{\mathrm{Te}}\sim 2.66$ a.u.). Brillouin-zone (BZ) integrations have utilized a 12-point *k* sample in the 1/16 irreducible wedge. Exchange and correlation effects have been treated via the Wigner interpolation formula.[14] The atomic Tl ($5d^{10}6s^26p^1$), Ga ($3d^{10}4s^24p^1$), and Te ($5s^25p^4$) states were treated as valence electrons in this study whereas the more tightly bound levels were included via a frozen-core approximation.

IV. RESULTS AND DISCUSSION

We show in Fig. 2 the AIPES spectra of $TlGaTe_2$ taken with He I and He II radiation and the calculated density of states (DOS) broadened with an energy-dependent Lorentzian and a Gaussian for the lifetime broadening and the instrumental resolution, respectively. We have assumed the full width at half maximum (FWHM) of the Lorentzian is equal to $0.1\times E_B$ as usual.[15] The integral background has been added to the broadened DOS. One can see five structures (labeled as A–E) in the He I spectrum. Two pronounced features A and C are not seen in the He II spectrum, and hence these structures are mainly attributed to Te $5p$ states, because the Te $5p$ cross section is dramatically reduced in going from He I to He II.[16] On the other hand, structures D and E at $E_B=5$–8 eV are seen in the He II spectrum, and hence these are assigned to Tl $6s$, and Ga $4s$ states. This assignment is confirmed by the muffin-tin projected partial DOS shown in Fig. 3. The He II spectrum, for which the cross sections of the Te $5p$, Tl $6s$ and Ga $4s$ states are not so different as those for the He I spectrum,[16] is in rather good agreement with the broadened total DOS.

Next, we show ARPES spectra of $TlGaTe_2$. In the following, $\mathbf{k}$ denotes the electron momentum in the solid and $\mathbf{k}_\parallel$ and $\mathbf{k}_\perp$ denote the components parallel and perpendicular to the (110) surface, respectively. (Thus $\mathbf{k}=\mathbf{k}_\parallel+\mathbf{k}_\perp$.) They are related to the momentum $\mathbf{k}'$ of the photoelectron in vacuum *via* $\mathbf{k}_\parallel=\mathbf{k}'_\parallel$, $|\mathbf{k}_\perp|=\sqrt{(2m/\hbar^2)[(\hbar^2\mathbf{k}'^2/2m)\cos^2\theta+V_0]}$ according to the free electron final-state model,[17] where θ is a

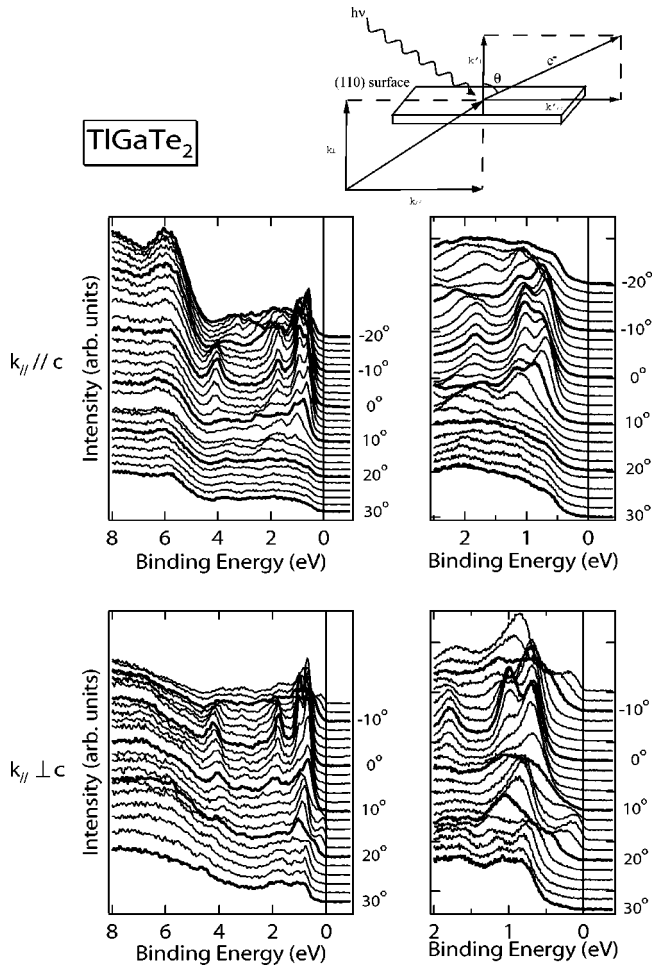

FIG. 4. ARPES spectra in wide region (left panels) and narrow region (right panels). Top: for $\mathbf{k}_{\|} \| c$. Bottom: for $\mathbf{k}_{\|} \perp c$ (b). Inset: measurement geometry showing the definition of $\mathbf{k}_{\|}$ and $\mathbf{k}_{\perp}$.

take-off angle of the photoelectron and V_0 is an inner potential. In the ''$\mathbf{k}_{\|} \| c$ arrangement,'' $\mathbf{k}_{\|}$ is parallel to the [001] direction, while in the ''$\mathbf{k}_{\|} \perp c$ arrangement,'' $\mathbf{k}_{\|}$ is parallel to the [110] direction. For both arrangements, $\mathbf{k}_{\perp}$ is parallel to the [110] direction. Figure 4 shows ARPES spectra taken at 22 K. The left panels show wide-range spectra measured in the $\mathbf{k}_{\|} \| c$ and $\mathbf{k}_{\|} \perp c$ arrangements. In spite of the chain structures running along the c axis, one can clearly see dispersive features for both arrangements, i.e., the band dispersions in $TlGaTe_2$ depend on the momentum not only parallel but also perpendicular to the chain direction. The right panels show spectra in a narrow energy range. The tail of some peak seems to overlap with the Fermi level for the $\mathbf{k}_{\|} \perp c$ arrangement. However, we consider that this is due to the finite energy resolution of $\sim$90 meV. Peaks do not cross the Fermi level.

The calculated band dispersion of $TlGaTe_2$ is shown in Fig. 5. The four bands from ~ -7 to ~ -4 eV evolve mainly from Tl 6s and Ga 4s states while the ten bands from ~ -4 to ~ 0 eV originate from Te 5p states. According to Fig. 5, the remaining two Te 5p bands are essentially split off from the ten occupied 5p bands to form a broad conduction band that overlaps Tl 6p and Ga 4p derived states.

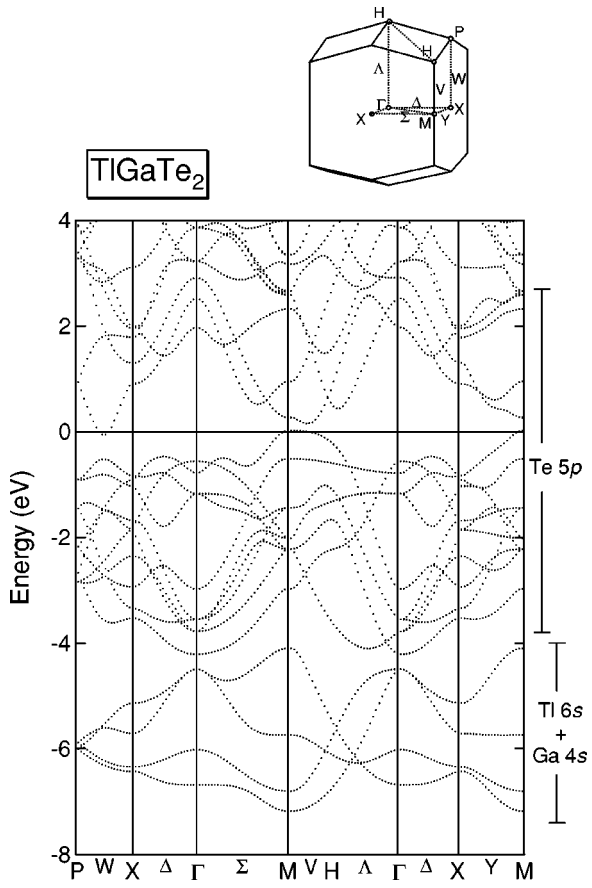

FIG. 5. Calculated band structure of $TlGaTe_2$.

Although the experimental results show that $TlGaTe_2$ is a semiconductor, the present calculations suggest that $TlGaTe_2$ is a semimetal which has a hole pocket at the M point and an electron pocket on the W line. This may be due to the inherent deficiency of LDA. If we assume the inner potential to be $\sim$12 eV as usual,[17] $\mathbf{k}$ is obtained as shown in Fig. 6. There is some ambiguity in the $\mathbf{k}_{\perp}$ value thus deduced because of the ''finite photoelectron lifetime.''[17] Thus ARPES spectra measure one-dimensional DOS integrated around this $\mathbf{k}_{\perp}$ for each $\mathbf{k}_{\|}$ and one can compare the $\mathbf{k}_{\|} \| c$ and $\mathbf{k}_{\|} \perp c$ ARPES dispersions a few eV from E_F with the calculated band structure along the X-W-P and X-Y-M symmetry lines, respectively. Figure 7 shows the results of such comparison between the experimental and calculated band dispersions within a few eV of E_F. The gray-scale plot is the second derivative of the experimental spectra. It seems that the plot shows a discontinuity at the X point. This may be due to a small misalignment of the surface normal off the emission plane. One can see several bands in the experimental result. The highest band disperses from just below E_F at the M point $(2\pi/a,0,0)$ to $\sim$1.0 eV below E_F at the P point. Other bands are seen around 0.8 eV at the M point, 1.0 eV at the X point, 1.8 eV at the X point, and so on. One finds that these bands have corresponding ones in the calculated result. In particular, the highest band representing the valence-band maximum at the M point seems to agree well with the calculated band.

The present LAPW results for $TlGaTe_2$ suggest a very

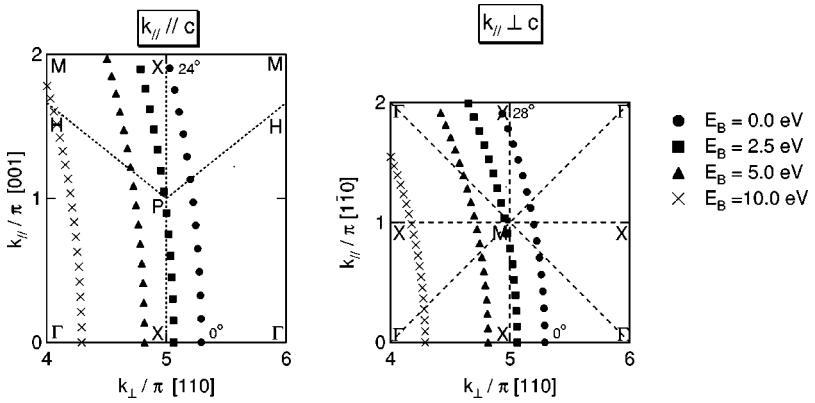

FIG. 6. Momentum of the photoexcited electron in the solid according to the free-electron final-state model.

simple picture of the underlying chemistry of this material. For example, assuming that the formal valence of both Tl and Ga is 1+, then the corresponding Te formal valence would be 1− and the Fermi level would be expected to occur near the top of the Te $5p$ bands, i.e., at an energy where, on average, ten of the 12 $5p$ bands are occupied. However, because of the very short Ga-Te bond length (~2.70 Å) within the $GaTe_4$ tetrahedra, the strong Ga $4s$–Te $5p$ interaction raises two of the 12 Te $5p$ bands above E_F, thereby opening a band gap at the $TlGaTe_2$ Fermi level. At the M point in Fig. 5, for example, these antibonding Ga $4s$–Te $5p$ bands occur at energies 0.9 and 2.3 eV, respectively. These unoccupied antibonding bands are overlapped by the Tl $6p$ and Ga $4p$ type states, producing the complicated conduction-band complex shown in Fig. 5.

Analysis of the LAPW wave function for the valence-band maximum at the M point reveals that ~50% of the weight consists of Te $5p_{x,y}$ and ~20% Tl $6s$. The interaction between the Tl $6s$ and Te $5p$ orbitals is analogous to that of the Ga-Te interaction, but is reduced by the fact that the Tl-Te bond length (~3.55 Å) is significantly larger than the corresponding Ga-Te value (~2.70 Å). As a result, this Tl-Te antibonding band falls at a lower energy and forms the valence-band maximum. It is clear that the electronic properties near E_F of p-type $TlGaTe_2$ are determined by a combination interchain Tl-Te interactions as well as intrachain Te-Te hopping. Although the Tl-Te bond length is rather large, these interchain interactions are enhanced by the fact that each Tl has eight Te nearest neighbors. As a result of these considerations, one can readily understand why the expected one-dimensional features in the $TlGaTe_2$ band structure are masked by interchain interactions.

We have also studied the temperature dependence of the ARPES spectra. The second derivatives of ARPES spectra taken at 22 and 300 K are shown in Fig. 8. One can see a

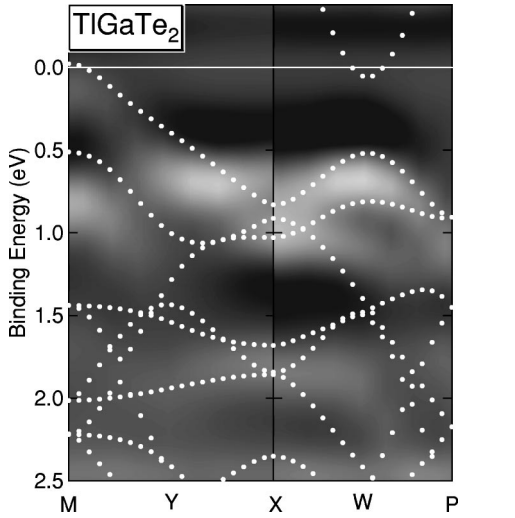

FIG. 7. Comparison of the ARPES spectra (gray-scale plot) with the calculated band structure (white dotted curves).

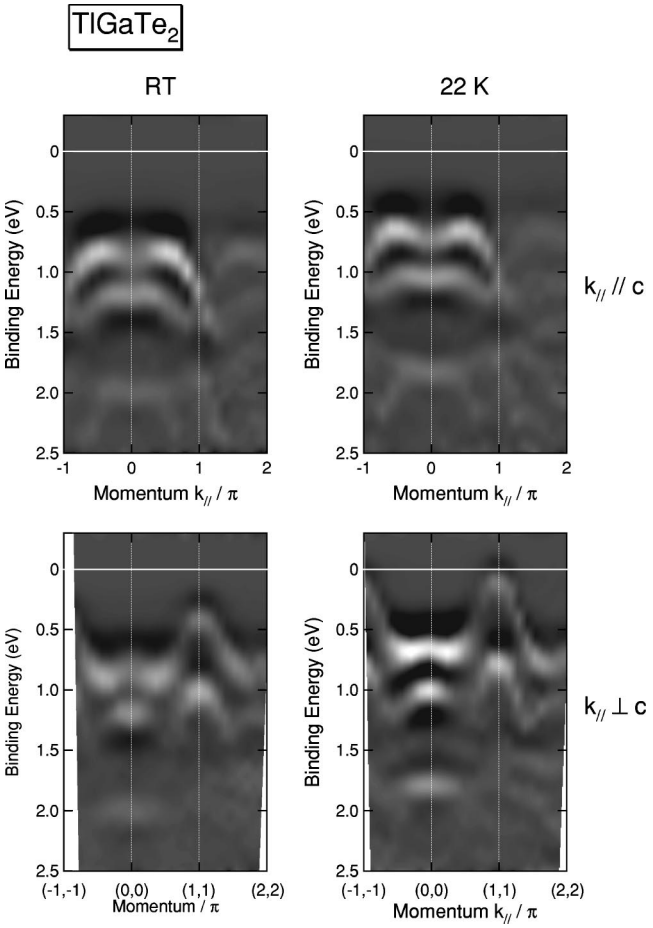

FIG. 8. Temperature variation (22 and 300 K) of the experimental band structure.

rigid shift of the whole spectral features toward lower binding energies when the temperature is decreased. This is most naturally explained by a downward shift of E_F. Since $TlGaTe_2$ is a *p*-type semiconductor,[3] at low temperatures E_F is pinned close to the accepter level which is usually located near the valence-band maximum. At high temperatures, E_F is shifted towards the middle of the band gap. This large shift of E_F may cause a large Seebeck coefficient in this material. In fact, large Seebeck coefficients have been reported for other TlSe-type compounds.[18] Some other changes have also been observed. The bandwidth is increased (by $\sim$0.1 eV) and the highest two bands are more clearly split (by $\sim$0.05 eV) at low temperature. Normal-incommensurate-commensurate structural phase transitions and a second-order phase transition have been reported[9] between these temperatures. Spectral changes may be related to these transitions, but we cannot draw a definite conclusion at this moment.

V. CONCLUSION

We have studied the electronic structure of $TlGaTe_2$ using photoemission spectroscopy and band-structure calculation. Comparison between the ARPES spectra and the calculated band structure is rather favorable. The top of the valence band is identified at the *M* point in the BZ and mainly consists of Te $5p$ states. From the strong band dispersion perpendicular to the *c* axis around the *M* point, it is concluded that $TlGaTe_2$ has a three-dimensional electronic structure in spite of the chain structure at least for the transport properties associated with the *p*-type carriers. The rigid shit of the band structure with temperature variation is explained by a shift of E_F expected for a *p*-type semiconductor. A possibility of a large Seebeck coefficient is suggested. The increase of the bandwidth and the splitting of the highest two bands at low temperature have been observed.

*Present address: Department of Physics and Electronics, University of Osaka Prefecture, Gakuen-cho 1-1, Sakai, Osaka, 599-8531, Japan.

[1] D. Müller, G. Eulenberger, and H. Hahn, Z. Anorg. Allg. Chem. **398**, 207 (1973).
[2] M. Hanias, A. N. Anagnostopoulos, K. Kambas, and J. Spyridelis, Phys. Rev. B **43**, 4135 (1991).
[3] M. P. Hanias and A. N. Anagnostopoulos, Phys. Rev. B **47**, 4261 (1993).
[4] M. K. Rabinal, S. Asokan, M. O. Godazaev, N. T. Mamedov, and E. S. R. Gopal, Phys. Status Solidi B **167**, K97 (1991).
[5] S. Abdullaeva and N. Mamedov, Turk. J. Phys. **17**, 568 (1993).
[6] N. T. Mamedov and A. M. Panich, Phys. Status Solidi A **117**, K15 (1990).
[7] F. M. Gashimzade and G. S. Orudzhev, Fiz. Tekh. Poluprovodn. **15**, 1311 (1981) [Sov. Phys. Semicond. **15**, 757 (1981)].
[8] F. M. Gashimzade and D. G. Guliev, Phys. Status Solidi B **131**, 201 (1985).
[9] V. A. Aliev, M. A. Aldzhanov, and S. N. Aliev, Pis'ma Zh. Éksp. Teor. Fiz. **95**, 418 (1987) [JETP Lett. **45**, 534 (1987)].
[10] G. D. Guseinov, A. M. Ramazanzade, E. M. Kerimova, and M. Z. Ismailov, Phys. Status Solidi **22**, K117 (1967).
[11] L. F. Mattheiss and D. R. Hamann, Phys. Rev. B **33**, 823 (1986).
[12] S. Kashida and N. Watanabe (unpublished).
[13] O. K. Andersen, Phys. Rev. B **12**, 3060 (1975).
[14] E. Wigner, Phys. Rev. **46**, 1002 (1934).
[15] K. Kobayashi, T. Mizokawa, K. Mamiya, A. Sekiyama, A. Fujimori, H. Takagi, H. Eisaki, S. Uchida, R. J. Cava, J. J. Krajewski, and W. F. Peck, Jr., Phys. Rev. B **54**, 507 (1996); J. Matsuno, T. Mizokawa, A. Fujimori, D. A. Zatsepin, V. R. Galakhov, E. Z. Kurmaev, Y. Kato, and S. Nagata, *ibid.* **55**, R15979 (1997).
[16] J.-J. Yeh and I. Lindau, At. Data Nucl. Data Tables **32**, 1 (1985).
[17] S. Hüfner, *Photoelectron Spectroscopy* (Springer-Verlag, Berlin, 1995).
[18] G. D. Guseinov, E. Mooser, E. M. Kerimova, R. S. Gamicov, I. V. Alekseev, and M. Z. Ismailov, Phys. Status Solidi **34**, 33 (1969).